Research Article | Vol. 28, No. 25 / 7 December 2020 / Optics Express 37708
Optics EXPRESS

Improvement of the signal-to-noise ratio in a low power self-mixing interferometer using a coupled interferometric effect

CARLOS YÁÑEZ* AND SANTIAGO ROYO

Centre for the Development of Sensors, Instruments and Systems, Universitat Politècnica de Catalunya - BarcelonaTech, Rambla Sant Nebridi 10, 08222 Terrassa, Spain
*carlos.rene.yanez@upc.edu

Abstract: We present experimental results of a low-emission self-mixing interferometer that uses a coupled interferometric effect to improve the signal produced by a vibrating target. This method is intended to be useful in applications where the target is prone to be damaged by high-intensity laser sources. The beam of a Fabry-Perot laser diode is split and ~21% of the original emission is used to measure the harmonic micro-displacements of the target using the self-mixing effect. A portion of the residual beam, which also carries the interferometric information related to the target displacement, is reinjected back into the laser cavity by means of a fixed reflector, causing a second interferometric phenomenon that improves the signal-to-noise ratio of the measurement by up to ~13 dB. A theoretical description of the phenomena is also proposed. Further, we apply this technique to the two most common self-mixing sensing schemes: internal photodiode and junction voltage. The reported results show good agreement with theory and prove the capability of the method to enhance the SNR in SMI schemes.

1. Introduction

Interferometers based on the well-known self-mixing effect are nowadays widely employed in applications for sensing variables such as displacement [1–3], distance [4,5], vibration [6], and velocity [4]. Soon after the invention of the laser by Theodore H. Maiman in 1960 [7], the first applications of laser feedback in metrology were reported; and the possibility to determine physical length and velocity by measuring changes in the optical path of a coherent source of light was described [8–10]. In 1968, Rudd [11] measured the Doppler shift occurring in the light-wave of a He-Ne laser focused onto a rotating mirror, reporting that the small portion of the light reinjected into the laser cavity after interacting with the moving object causes a modulation in the optical output power (OOP) equivalent to the Doppler frequency. Later on, Shinohara *et al.* [12] named this phenomenon the Self-Mixing effect.

A self-mixing interferometer (SMI), also known as optical feedback interferometer (OFI), is a self-aligned system that can be easily implemented using a single lens to direct a laser beam at a moving target and to collect a portion of the reflected light to be injected back into the laser cavity, causing a modulation in the frequency and amplitude of the OOP equivalent to the fringes found in a Michelson or Mach-Zehnder interferometer.

With the appearance of laser diodes (LD) that have a photodetector (PD) integrated in the same packaging, an external PD is not even required for monitoring the changes in the OOP. Moreover, as explained in [13], it is also possible to acquire the SMI signal by measuring the changes in the junction voltage (JV) of the LD, so a PD is not essential in this type of interferometers.

Recently, several biomedical solutions based on SMI have been described [14]. These developments can be potentially implemented in daily health treatments or life science studies; however, in some cases, important shortcomings must be addressed before reaching such ideal scenario. One of the most critical considerations to be managed is laser safety, related to the eye

#405997 https://doi.org/10.1364/OE.405997
Journal © 2020 Received 21 Aug 2020; revised 8 Oct 2020; accepted 23 Oct 2020; published 1 Dec 2020

Optics EXPRESS

or the skin, very specially when continuous, focused beams are involved, such as in the case of microscopy.

At an early stage of laser development, researchers recognized the potential risks of this intense beam of light, and two scientific papers on the subject were published as early as 1961, Solon *et al.* [15] described the hazardous implications of such an extremely collimated beam with a high degree of monochromaticity, and Zaret *et al.* [16] experimented with thermal lesions produced by a pulsed optical maser (laser) in the retina and iris of a rabbit, concluding that this device could cause significant damage to the human eye too.

Nowadays, safety should be considered an integral part of using laser technology. The International Commission on Non-Ionizing Radiation Protection (ICNIRP), the American National Standards Institute (ANSI), and the International Electrotechnical Commission (IEC), jointly define the Exposure Limit Values (ELV) (also known as Maximum Permissible Exposure – MPE – values) that stipulate the theoretical limits between safe and potentially harmful level of laser exposure in the eye or the skin [17]. Therefore, as the laser emission must be restricted for safety reasons, in the specific case of SMI applications this compromises the amount of photons that reach the laser cavity after being reflected from a diffusive target, negatively affecting the signal-to-noise ratio (SNR) of the measurements, critical for accurate fringe detection.

In this paper, we propose a new method that improves the SNR of self-mixing configurations in which the optical emission reaching a sample needs to be intentionally limited to reduce the risk of causing damage or alterations on the target. We designed a low-intensity self-mixing interferometer dividing the laser beam produced by an 830 nm Fabry-Perot laser diode by means of a 30:70 beam splitter. The resulting low-intensity beam was used to measure the harmonic motion induced to a target by a piezo-electric actuator; however, as explained before, as far as the back-reflected light reaching the laser cavity after a round-trip is also limited by the very nature of the system, the SNR of the SMI signal was compromised to some extent. We overcome this issue by using the residual part of the original beam as a signal amplifier through a novel coupled interferometric effect. As stated in [18], the SMI information is carried throughout the entire beam and can be picked up everywhere; this means that regardless of whether the secondary beam is not in contact with the target, it also exhibits the modulation of the OOP caused by the interaction of the target with the measuring beam. Therefore, by reinjecting a portion of this residual beam into the laser cavity, we cause an additional interferometric phenomenon between the two optical paths, which allows us to significantly improve the SNR of the resulting SMI signal.

Although double external cavity configurations based on SMI have been reported before [19–22], to the best of our knowledge there have been no reports of the use of a double interferometric effect between the two channels to improve the SNR.

This paper is organized as follows: Section 2 explains the theoretical framework and materials for the experiments. In Section 3 we introduce a general approach of the proposed technique with two proof-of-concept experiments, which demonstrate the effectiveness of the method applied to both the PD and JV detection schemes; then, we present an integration of our scheme with an optical microscope, to simulate a tool intended to measure the vibration of microbiological samples (*e.g.*, living cells) under a given stimulus. This application may be of special interest in biomedicine [23–27], botany [28] and/or zoology [29]. Finally, conclusions will be drawn in Section 4.

2. Material and methods

2.1. Theoretical approach

As with any well-stablished technique, the theory behind self-mixing interferometry has been extensively documented before. The most common models devised to explain the self-mixing effect with a single external target are the Lang and Kobayashi rate equations [30] and the

Optics EXPRESS

three-mirror Fabry-Perot cavity model by Petermann [31]. Based on these analysis, external dual cavity models have been also derived [19–22]. Although an exhaustive theoretical review is beyond the scope of this article, we introduce a simple derivation of the coupled SMI effect based on the work of Petermann and the dual-channel approach presented by Lu *et al.* [22].

In Fig. 1 a scheme of the three mirror Fabry-Perot approach is depicted. For simplicity, only the first round-trip along the entire cavity is considered.

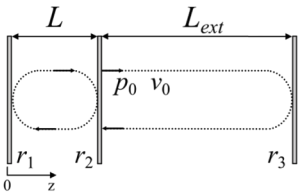

Fig. 1. Schematics of the three mirror configuration for a semiconductor laser with external optical feedback: L, length of the laser cavity; L_{ext}, length of the external cavity; r_1, r_2, amplitude reflection coefficients of the laser cavity mirrors; r_3, amplitude reflection coefficient of the surface of the external target; p_0, optical output power without feedback; v_0, emission frequency of the free-running laser; z, propagation axis.

The active cavity of a semiconductor laser is formed by two mirrors with an amplitude reflection coefficient r_1, r_2, respectively; this optical resonator of length L amplifies an electric field until reaching a stable lasing state. The released coherent beam, with emission frequency v_0 and optical power p_0, travels along the propagation axis z and interacts with the rough surface of an external target acting as a third mirror with an amplitude reflection coefficient r_3, thus forming a secondary cavity of length L_{ext}. A small portion of the optical beam is back-reflected by the third mirror and reinjected into the laser cavity, recombining with the resonant modes of the laser and causing a substantial variation in the OOP. If the target is in motion, the period between two of these variations is due to a target displacement of half wavelength [19].

If a single reflection is considered (*e.g.*, due to a diffusive target surface or weak optical feedback) the coupling coefficient k indicates the quantity of reinjected light coupled into the laser cavity:

$$k = \frac{r_3}{r_2}(1 - |r_2|^2). \tag{1}$$

The effectiveness of the optical feedback to change the intrinsic behavior of the laser is given by the C factor [32]:

$$C = k\frac{\tau_{Lext}}{\tau_L}\sqrt{1+\alpha^2}. \tag{2}$$

where $\tau_{Lext} = 2L_{ext}/c$ and $\tau_L = 2L\mu_e/c$ are the round-trip time of flight in the external and internal cavity respectively, c stands for the speed of light in vacuum, μ_e is the effective refractive index inside the laser cavity, and α is the linewidth enhancement factor [33].

The field reflected by r_2 and the reinjected field coming from r_3 can be treated as a single term. This simplification allows r_2 and r_3 to be combined into an equivalent effective amplitude reflection coefficient r_{eq}:

$$r_{eq} = r_2 + (1 - |r_2|^2)r_3 \exp(-j2\pi v\tau_{Lext}). \tag{3}$$

here, v is the emission frequency of the laser with optical feedback.

The steady state oscillation within the laser cavity requires that all the fields inside the cavity stays constant in amplitude, and the round-trip phase shift inside the cavity $2\beta L + \varphi_r = 2\pi m$ (phase condition); being m an integer, $\beta = 2\pi v_0\mu_e/c$, and $\varphi_r = 0$ when there is no feedback.

Optics EXPRESS

For weak optical feedback (*i.e.* $|r_3| \ll |r_2|$), the phase shift of the reflection coefficient is:

$$\varphi_r = k \sin(2\pi v \tau_{Lext}). \tag{4}$$

being $k \ll 1$.

The amplitude reflection coefficient in Eq. (1) can then be expressed as:

$$|r_{eq}| = r_2(1 + k\cos(2\pi v \tau_{Lext})). \tag{5}$$

The change in the round-trip phase compared to $2\pi m$ that occurs due to optical feedback can be written as:

$$\Delta\phi_L = 2\pi\tau_L(v - v_0) + C\sin(2\pi v\tau_{Lext} + \arctan\alpha). \tag{6}$$

$\Delta\phi_L$ is commonly referred to as the excess phase. Emission frequencies that satisfy the phase condition are characterized by $\Delta\phi_L = 0$.

The OOP with feedback, p, can be expressed as a function of the OOP without feedback p_0 [34]:

$$p = p_0(1 + \zeta\cos(2\pi v\tau_{Lext})). \tag{7}$$

where $\zeta = exp(-\pi\delta v\tau_{Lext})$ is the modulation parameter. Here, δv is the spectral linewidth of the LD with feedback, that explains the autocorrelation function of the normalized field due to white frequency noise.

A dual-channel SMI configuration can be thought of as two independent single-channel interferometers sharing the same source and detector. In fact, if a target is placed in one of its optical paths and the other allows a free-running emission, the system will act as a regular single-channel self-mixing interferometer. Hence, the choice of which external cavity is the target and which is the fixed cavity, depends entirely on the split ratio of the beam splitter.

Considering that both channels are occupied by two reflective surfaces, the three mirror model becomes a four mirror scheme, as shown in Fig. 2.

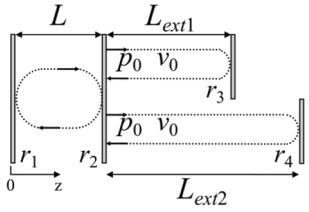

Fig. 2. Schematics of a dual-channel self-mixing interferometer.

Therefore, the same theoretical analysis allows to rewrite the change in the round-trip phase, $\Delta\phi_L$, taking into consideration the two channels:

$$\begin{aligned}\Delta\phi_L = 2\pi\tau_L(v - v_0) + \eta_1 C_1 \sin(2\pi v\tau_{Lext1} + \arctan\alpha) + \\ \eta_2 C_2 \sin(2\pi v\tau_{Lext2} + \arctan\alpha)\end{aligned}. \tag{8}$$

C_1 and C_2 can be easily obtained from Eq. (1) and Eq. (2), τ_{Lext1} and τ_{Lext2} represent the round-trip delay due to the length of each external cavity and η_1 together with η_2 stands for the split ratio of the beam splitter, so $\eta_1 + \eta_2 = 1$.

The modulation in the OOP due to the influence of the two channels can then be expressed as:

$$p = p_0[(1 + \eta_1\zeta_1\cos(2\pi v\tau_{Lext1})) + (1 + \eta_2\zeta_2\cos(2\pi v\tau_{Lext2}))]. \tag{9}$$

where $\zeta_1 = exp(-\pi\delta v\tau_{Lext1})$ and $\zeta_2 = exp(-\pi\delta v\tau_{Lext2})$.

Optics EXPRESS

The sum of both terms in Eq. (9) leads to maximum intensity in p when the signals in channel 1 and channel 2 are in phase with each other; on the contrary, when they are in antiphase, the signals cancel each other and p reaches a marginal value. In Section 3, simulations of the theoretical model are presented and contrasted with actual measurements.

2.2. Low power self-mixing interferometer with dual external cavity

A beam splitter with 30:70 split ratio (Thorlabs, BSS11R) was used to implement the dual external cavity setup. Note that this ratio can be adjusted in real-life applications depending on the laser safety requirements of the sample. A diagram of our setup is presented in Fig. 3.

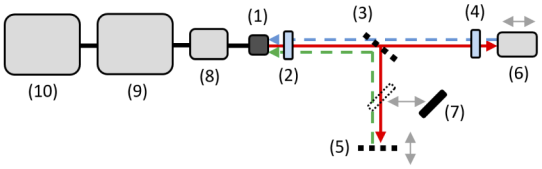

Fig. 3. Diagram of the experimental setup: 1, LD; 2, collimating lens; 3, 30:70 beam splitter; 4, focusing lens; 5, 50:50 beam splitter; 6, piezo-electric actuator; 7, light trap; 8, laser driver/data acquisition card; 9, oscilloscope; 10, personal computer.

An 830 nm GaAlAs Fabry-Perot laser diode (Opnext, HL8338MG) was mounted in a collimation system (Thorlabs, LT220P-B) and its beam is divided by the beam splitter, the resulting low-intensity beam (*i.e.*, the sensing beam) was directed to a focusing lens (Optem, 35-00-02-000) that focus the beam over the moving surface of a piezo-electric actuator (PI, P753.2) (*i.e.*, the active cavity). The high-intensity beam forms a fixed external cavity with a 50:50 beam splitter (Thorlabs, BSW11) mounted in a high-resolution linear actuator (PI, M-227), that allows to adjust the fixed cavity length with a theoretical resolution of 0.0035 µm and a minimum incremental motion of 0.05 µm. Note that the 50:50 beam splitter is used instead of a flat mirror so as not to saturate the laser cavity with excessive feedback. The fixed cavity length was initially established as ~30 cm, and the length of the active cavity as ~25 cm; however, the initial distance in either of the two optical paths can be considered irrelevant. A light trap made with a light absorbing black-out material (Edmund Optics) allowed to cancel the effect of the fixed cavity for comparison when needed.

The LD was fed with its theoretical minimum threshold current of 20 mA to obtain the lowest possible OOP, which was measured in front of the collimating lens with a digital optical power and energy meter (PM100D, Thorlabs), resulting in ~4.05 mW. After the beam splitter, the OOP in the fixed cavity was ~2.65 mW and in the focal point of the focusing lens ~0.87 mW. Thus, the energy that reaches the target is ~21% of the original emission. A variation of ±0.04 mW due to changes in the temperature of the LD, losses along the optical path, and other not critical external factors should be considered.

As explained before, there are two main detection schemes used in SMI to measure the modulation in the OOP caused by optical feedback: the PD scheme and the JV scheme. This last configuration is commonly employed when the laser diode lacks a monitoring PD, as in some Vertical-Cavity Surface-Emitting (VCSEL) LDs [13]. For that reason, we decided to conduct experiments with both detection schemes using the same HL8338MG LD, which has a built-in PD, so as to confirm that our method can be applied indifferently to both configurations. For that reason, two laser driver/data acquisition cards were designed, one to be used with the PD arrangement, and other for the JV scheme. All other elements in the setup remained the same in the experiments for comparison purposes. The frequency range of the system is limited by the cutoff frequencies of the operational amplifiers used for the amplification of the SMI signal obtained from the internal photodiode and the junction of the LD and the noise filters, resulting

Optics EXPRESS

in 0.5 Hz – 1.2 Mhz. The SMI signal acquired by the data acquisition card was digitalized by an oscilloscope (Pico, Picoscope 4227) and transmitted to a personal computer through the USB 2.0 protocol.

It is well-known that in any SMI setup the interferometric information is carried throughout the entire beam and can be picked up everywhere [18], meaning that the portion of the beam reinjected back from the fixed cavity is actually an output of the interferometer in the active cavity. Hence, the OOP of a system under double optical feedback is expected to undergo a double sort of modulation regardless of whether the target in the fixed cavity remains static. This coupled interferometric effect occurs mainly due to constructive or destructive interference from the recombined light coming from each of the channels. Note that this effect occurs necessarily in every conventional interferometer, where part of the light always comes back to the emitting laser, leading to optical feedback effects.

The amplitude condition in the steady state demands that there is no destructive interference between the fields inside the cavity, so the accumulated phase of all the fields during a round-trip must be equal to $2\pi m$. On the other hand, a difference of phase of $(2m + 1)\pi/2$ leads to a minimum amplitude in the intensity (*i.e.* the wavefronts are in antiphase). If we consider that both reinjected fields have the same amplitude, complete destructive interference arises when the difference between L_{ext1} and L_{ext2} is $(2m + 1)\lambda/4$; therefore vanishing the self-mixing signal. Conversely, if the difference in the external paths is $m\lambda/2$, the waves will reinforce each other due to constructive interference, improving, thus, the SNR of the interferometric system.

3. Experiments and results

As explained above, to obtain the maximum amplitude of the SMI signal in this dual-channel system, a difference of $m\lambda/2$ between L_{ext1} and L_{ext2} is required, rather than a specific distance on any of the optical paths. This means that both the initial position of the target and that of the fixed cavity are irrelevant, and depend on other considerations (*e.g.*, the overall compactness of the setup, the reflectivity of the surfaces involved, the characteristics of the propagation medium, and so on). In our initial configuration, $L_{ext1} \approx 25$ cm is the active cavity and $L_{ext2} \approx 30$ cm is the fixed cavity.

It is important to mention that a complete signal loss was consistently observed when the beam reflected from the fixed cavity was precisely aligned back into the laser cavity, due to excessive feedback levels. For that reason, the 50:50 beam splitter (acting as fixed cavity) was adjusted in such a way that the reflected beam does not enter directly through the center of the collimating lens, but halfway between the outer edge and the center.

The initial calibration of the setup consisted of moving the fixed cavity 0.05 µm each time, until finding the point where the two SMI signals are in phase inside the laser cavity. As seen in Fig. 4, there is a point where the two signals are in antiphase and cancel each other, Fig. 4(a). From here, as the length of the fixed cavity is progressively varied, two superimposed signals are observed until reach the difference of $m\lambda/2$, at which the two signals become in phase, thereby causing the improvement in the SNR, Fig. 4(d).

Based on the theoretical derivation presented in subSection 2.1, a simulation of the calibration process is presented in Fig. 5. In concordance with the actual process presented in Fig. 4, the simulated SMI signal corresponds to the measurement of a sinusoidal displacement of 5 µm in amplitude and 2 Hz in frequency. In Fig. 5(a) the difference between L_{ext1} and L_{ext2} is $(2m+1)\lambda/4$; the optimal difference of $m\lambda/2$ is represented in Fig. 5(d); in Figs. 5(b) and 5(c) is simulated a difference of $m\lambda/2.57$ and $m\lambda/2.49$ respectively. In all cases $m = 2$. A white Gaussian noise of 16 dB was added to the SMI signal in each channel, consistent with the real measurements. As can be observed, there is a remarkable correspondence between the simulations and the results obtained experimentally.

Optics EXPRESS

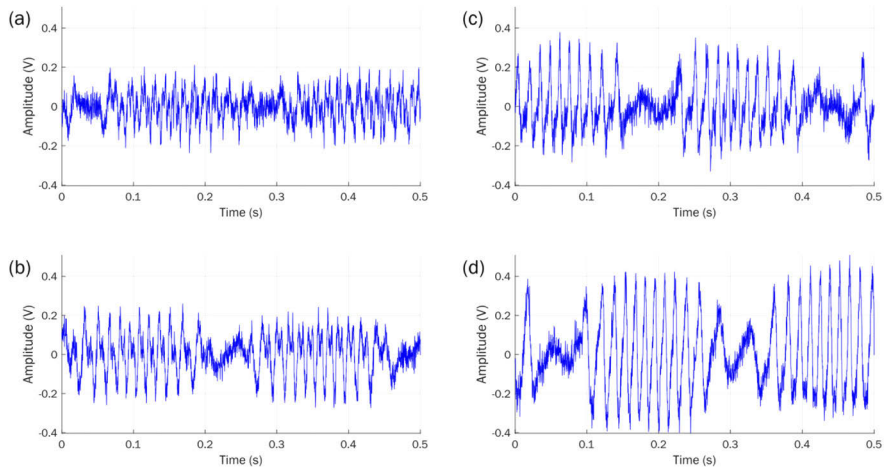

Fig. 4. Experimental calibration process for the measurement of a sinusoidal displacement with an amplitude of 5 µm and a frequency of 2 Hz. From (a), where both SMI signals are in antiphase, to (d), where the signals become in phase and the improvement of the SNR is optimal.

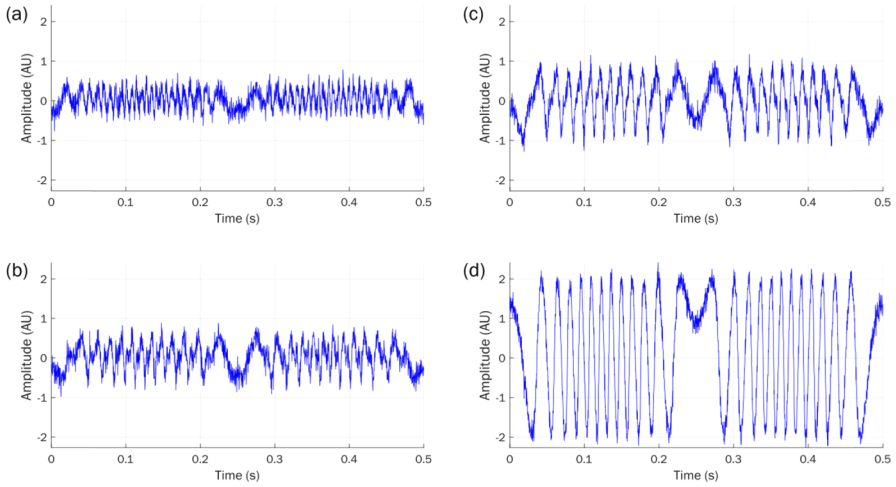

Fig. 5. Simulation of the main steps of the calibration process for the measurement of a sinusoidal displacement of 5 µm in amplitude and 2 Hz in frequency.

3.1. Proof-of-concept experiments

Once the dual-channel interferometer has been properly calibrated, we fed the piezo-electric actuator, acting as a target, first with a sawtooth signal with an amplitude 5 µm and 7 Hz in frequency, and later with a sinusoidal wave with the same parameters. Two different measurements were registered for each signal, one using the fixed cavity, and other blocking this path with the light trap, as illustrated in Fig. 3. The results obtained for the PD detection scheme are presented in Fig. 6. As it can be seen, using the coupled interferometric effect, the experimental SNR improvement achieved was ~9 dB.

In Fig. 7, the results obtained for the JV detection scheme show that when the coupled interferometric effect is not used, the loss of fringes in the SMI signal is significant for the sinusoidal movement; on the other hand, the improvement in the SNR provided by our method

Optics EXPRESS

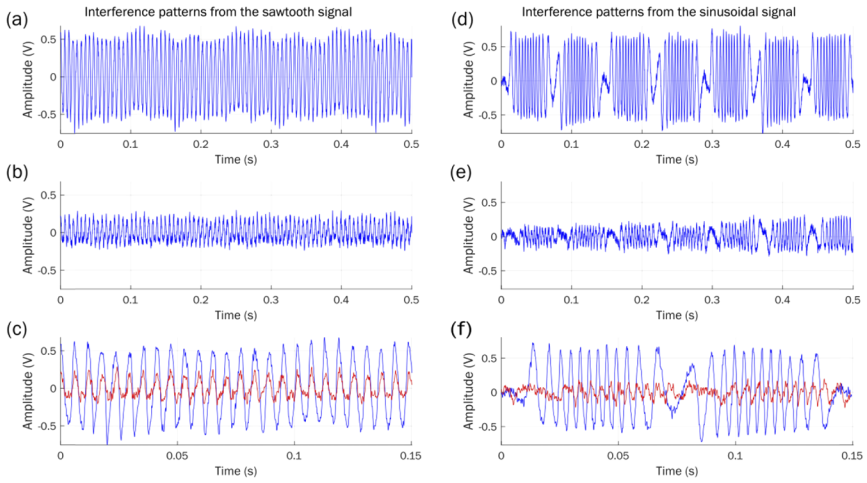

Fig. 6. SMI signals obtained from sawtooth and sinusoidal displacements using the PD detection scheme. (a) and (d) show the results of the coupled interferometric method; (b) and (e) show the results obtained without the fixed cavity; in (c) and (f) a comparison is presented. The SNR improvement was calculated as ~9 dB.

allows to accurately identify all the interferometric fringes related to the target displacement. Here, we calculated an experimental signal improvement of ~6 dB on average.

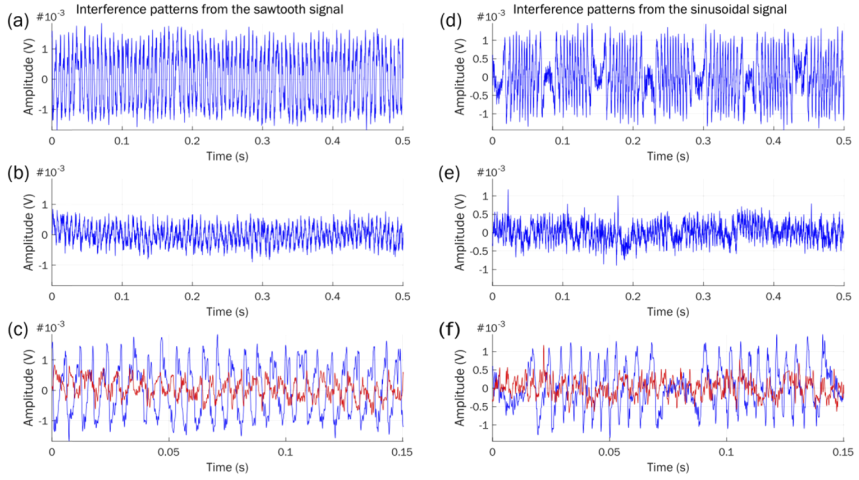

Fig. 7. Results obtained for the JV detection scheme: (a), (d), the coupled interferometric method; (b), (e), the single-channel SMI scheme; (c), (f), a comparison showing an improvement of ~6 dB in the SNR.

This last result is relevant, as it demonstrates that our coupled interferometric method successfully contributes with a significant improvement of the SMI signal, when a low-intensity laser source is employed. As stated by Donati in [35], in the JV detection scheme the SNR is limited by the relatively small dynamic resistance found in parallel to the junction of the LD, therefore, it provides less performance (up to ~-50 dB) compared with the PD detection approach. Hence, the proposed method can be used to improve the SNR in applications where the JV scheme is required.

Optics EXPRESS

Next, we intend to demonstrate that the SMI signal obtained from our low power interferometer and the proposed coupled interferometric effect has an amplitude equivalent to a single channel SMI setup in which the entire laser emission reaches the target. For this, we compared the amplified signals obtained previously from sawtooth and sinusoidal displacements using the JV configuration, with two measurements acquired from identical displacements in a JV setup, but using just a collimating and a focusing lens (Fig. 8), therefore allowing the entire beam of ~4.05 mW to reach the target surface.

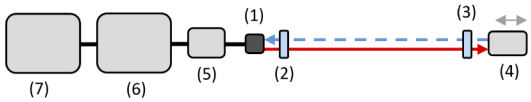

Fig. 8. Diagram of the setup for the measurements using the entire laser emission: 1, LD; 2, collimating lens; 3, focusing lens; 4, piezo-electric actuator; 5, laser driver/data acquisition card; 6, oscilloscope; 7, personal computer.

As can be seen in Fig. 9, the amplitude of the SMI signal obtained using our method is indeed equivalent in amplitude to that obtained with the entire laser emission, but the optical power reaching the target surface was reduced by ~79%.

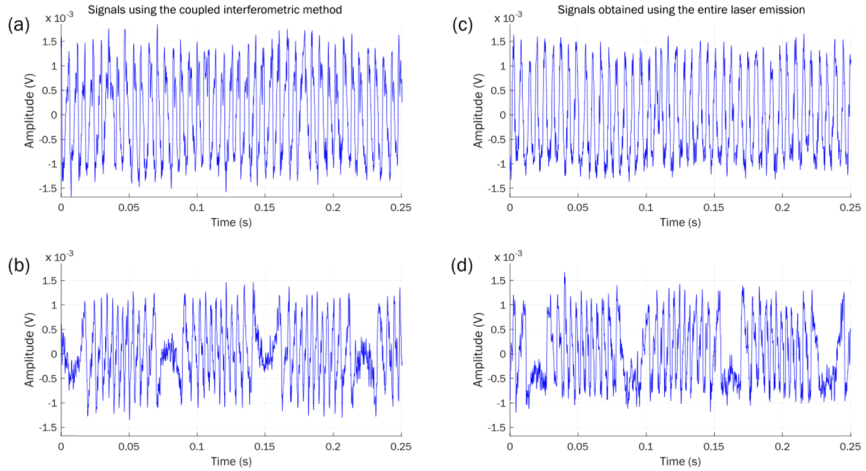

Fig. 9. Comparison between two SMI signals obtained from sawtooth [(a) and (c)] and sinusoidal [(b) and (d)] displacements using the JV detection scheme. (a), (b), with the coupled interferometric method; (c), (d), using the entire optical power of a single channel setup.

3.2. *Practical implementation of the method*

The measurement of the micrometric displacement of particles in medicine or life sciences is certainly a potential field of application for our method. This last experiment was intended to be a close-to-real life application of the proposed technique, to some extent similar to conditions described in [23–29], where, depending on each situation, the radiant exposure must be considered (and controlled) so as not to damage the sample under study.

We modified an optical microscope so we were able to integrate our low power interferometer within its optical path, as illustrated in Fig. 10. A 50x microscope objective with a numerical aperture of 0.55 (Optem, LWD, M-Plan Apo) was used to focus the sensing beam on the sample,

Optics EXPRESS

which can also be illuminated with a white light source that allows a digital camera (Canon, EOS 1000D) to be used as a real-time viewfinder.

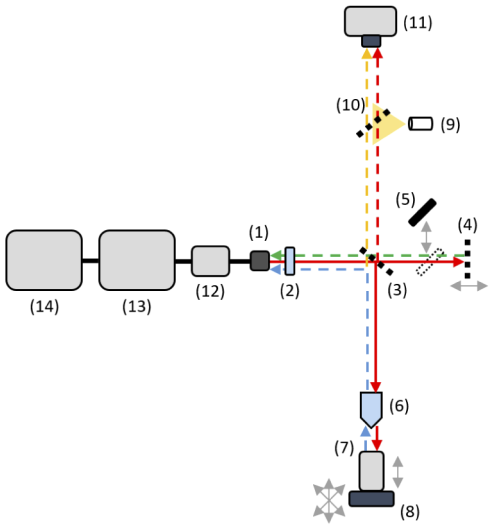

Fig. 10. Diagram of the setup used to analyze the displacement of microparticles: 1, LD; 2, collimating lens; 3, 30:70 beam splitter; 4, 50:50 beam splitter; 5, light trap; 6, 50x microscope objective; 7, piezo-electric actuator; 8, 3D stage; 9, white light source; 10, 50:50 beam splitter; 11, digital camera; 12, laser driver/data acquisition card; 13, oscilloscope; 14, personal computer.

The OOP measured at the focal point of the microscope objective was ~0.89 mW. According to [17], the laser beam from a device for the intended applications must reach the skin (the biological sample used as a reference for the laser safety classification, together with the human eye) with a maximum optical power of 3.3 mW, to meet the Class 3R requirements for non-visible IR laser equipment. This value is easily achieved with our low power SMI configuration, unlike a single channel setup that uses the entire ~4.05 mW of the laser source as sensing beam.

We used SiO_2 microspheres of 9-13 μm in diameter (Sigma-Aldrich) diluted in medical grade water based lubricant (HR Pharmaceuticals) to simulate a typical in vitro cell culture or living microorganisms in a test solution. The petri dish containing the sample was mounted over the piezo-electric actuator (in this experiment a PI-P753.3 actuator was used). The highly reflective surface of the actuator was covered with a portion of the light absorbing black-out material, and was positioned under the microscope objective with an inclination of ~2° to avoid, as much as possible, direct reflections from its surface. Afterwards, using a mechanical 3D stage we focused the measuring beam over a single microsphere within the sample. Figure 11.

According to [17], the safety exposure limit in skin at 830 nm is 300 seconds, yet it can vary depending on the biological sample in a real situation. We set the exposure time limit for each measurement as 10 seconds, a reasonable value if we consider the sample as a cell culture.

We induced a sinusoidal movement on the sample with amplitude of 1.9 μm (equivalent to 0.5 Vpp in the piezo-electric actuator) and 5 Hz in frequency. Similarly to previous results, in Fig. 12 the SMI signal obtained using the coupled interferometric effect and the PD sensing scheme is presented, and can be compared with the SMI signal obtained when the fixed cavity is blocked using the light trap. A basic fringe-counting algorithm was used over the amplified signal to reconstruct the displacement induced in the microsphere sample. Please note that there exist more sophisticated algorithms capable of reconstructing displacements in SMI applications [36];

Optics EXPRESS

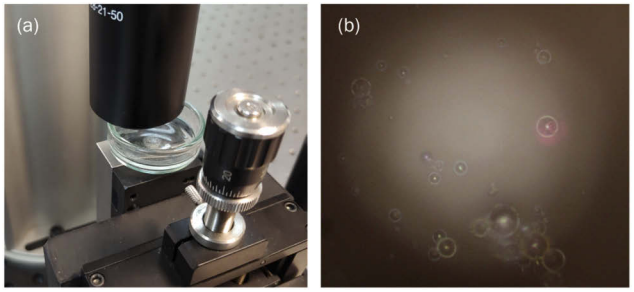

Fig. 11. The focusing system of our setup is shown in (a), and an example of the images displayed by the viewfinder, that allow the sensing beam to be precisely focused on a single microsphere, is presented in (b).

however, we used the fringe counting technique to limit the theoretical clarifications, since the basic principle can be easily understood from [6].

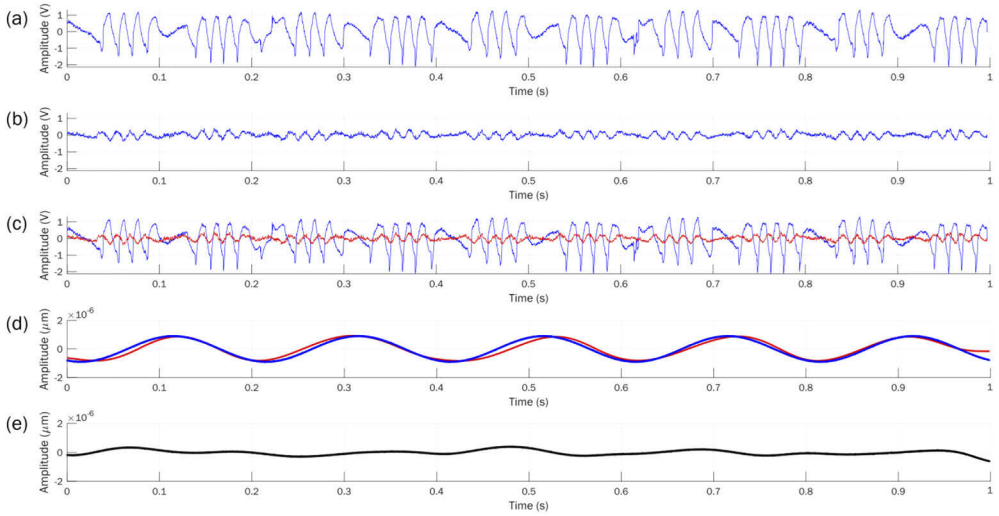

Fig. 12. Measurements obtained from the harmonic displacement induced to a single microsphere: (a), SMI signal obtained using the proposed coupled interferometric method; (b), signal obtained using the single-channel SMI scheme; (c), a comparison between the two signals; (d), in blue, the sinusoidal movement induced to the target, in red, the reconstruction obtained using a basic fringe-counting algorithm; (e), Mean absolute error (137 nm in average).

As clearly shown in Fig. 12(c), the SNR was dramatically improved by ∼13 dB, while the OOP was reduced by ∼79% of the original emission, thus reducing the risk of damaging the sample under study.

The error exhibited in the reconstruction of the microsphere displacement, which is 137 nm in average (7.2%), can be attributed, mainly, to the low number of interferometric fringes produced by the 1.9 μm displacement and the laser wavelength (830 nm). Furthermore, the viscosity of the water based lubricant where the microspheres are embedded may vary, to some extent, the displacement induced by the piezo-electric actuator to the microspheres.

Optics EXPRESS

4. Conclusions

We have presented a new method aimed to improve the SNR of a low power interferometer based on the well-known self-mixing effect. This interferometer was built using a Fabry-Perot laser diode as light source, and the theoretical threshold current of 20 mW was used to obtain the lowest possible optical output power (~4.05 mW). Then, a beam splitter of 30:70 allowed obtaining a low-intensity beam of ~0.89 mW used to measure the displacement of a target prone to be damaged by high-intensity light. The residual beam of ~2.6 mW in the second optical path was used as a fixed external cavity that allowed us to significantly improve the SNR of the SMI signal obtained as a result of the movement of the target. We found that this signal enhancement occurs due to a coupled interferometric effect that arises in the laser cavity mainly due to constructive or destructive interference from the recombined light coming from the two optical paths. For this enhancement to occur, a difference between the two optical paths of $\sim m\lambda/2$ must be established, to avoid the undesirable effect of having destructive interference or two superimposed SMI signals.

The experiments presented in this paper demonstrate that without the fixed external cavity, the low-emission interferometer was not reliable enough to accurately infer the target displacement, in special under the SMI junction voltage scheme.

A potential use of this technique in biomedical applications was also presented. Here, we combined the low-emission interferometer with an optical microscope to investigate the harmonic displacement induced to SiO2 microspheres of 9 -13 μm in diameter. This experiment aimed to simulate the measurement of the displacement of living cells or microorganisms. Our results demonstrated that the presented coupled interferometric method is able to measure with high SNR under faint illumination conditions. Such a setup has direct applications in areas such as medicine, entomology, botany, cytopathology, and other health sciences.

Funding

Consejo Nacional de Ciencia y Tecnología (472102); Ministerio de Economía y Competitividad (FIS2017-89850R).

Disclosures

The authors declare no conflicts of interest.

References

1. K. Zhu, B. Guo, Y. Lu, S. Zhang, and Y. Tan, "Single-spot two-dimensional displacement measurement based on self-mixing interferometry," Optica **4**(7), 729–735 (2017).
2. Y. Zhao, B. Zhang, and L. Han, "Laser self-mixing interference displacement measurement based on VMD and phase unwrapping," Opt. Commun. **456**, 124588 (2020).
3. D. Guo, L. Shi, Y. Yu, W. Xia, and M. Wang, "Micro-displacement reconstruction using a laser self-mixing grating interferometer with multiple-diffraction," Opt. Express **25**(25), 31394–31406 (2017).
4. M. Norgia, D. Melchionni, and A. Pesatori, "Self-mixing instrument for simultaneous distance and speed measurement," Opt. Lasers Eng. **99**, 31–38 (2017).
5. D. Wang, J. Zhou, C. Wang, J. Wang, H. Deng, and L. Lu, "Measurement of the absolute distance inside an all fiber DBR laser by self mixing technique," Proc. SPIE **10250**, 1025022 (2017).
6. M. Usman, U. Zabit, O. D. Bernal, G. Raja, and T. Bosch, "Detection of multimodal fringes for self-mixing-based vibration measurement," IEEE Trans. Instrum. Meas. **69**(1), 258–267 (2020).
7. T. H. Maiman, "Stimulated optical radiation in ruby," Nature **187**(4736), 493–494 (1960).
8. C. Hilsum and P. G. R. King, "Some demonstrations of the properties of optical masers," Contemp. Phys. **4**(6), 435–444 (1963).
9. P. G. R. King and G. J. Steward, "Metrology with an optical maser," New Sci. **17**, 180 (1963).
10. P. G. R. King and G. J. Steward, *Apparatus for measurement of lengths and of other physical parameters which are capable of altering an optical path length*, U.S. patent 3,409,370 (1968).
11. M. J. Rudd, "A laser Doppler velocimeter employing the laser as a mixer-oscillator," J. Phys. E: Sci. Instrum. **1**(7), 305723 (1968).

Optics EXPRESS

12. S. Shinohara, A. Mochizuki, H. Yoshida, and M. Sumi, "Laser Doppler velocimeter using the self-mixing effect of a semiconductor laser diode," Appl. Opt. **25**(9), 1417–1419 (1986).
13. Y. L. Lim, K. Bertling, P. Rio, J. R. Tucker, and A. D. Rakic, "Displacement and distance measurement using the change in junction voltage across a laser diode due to the self-mixing effect," Proc. SPIE **6038**, 60381O (2005).
14. J. Perchoux, A. Quotb, R. Atashkhooei, F. J. Azcona, E. E. Ramírez-Miquet, O. Bernal, A. Jha, A. Luna-Arriaga, C. Yañez, J. Caum, T. Bosch, and S. Royo, "Current developments on optical feedback interferometry as an all-optical sensor for biomedical applications," Sensors **16**(5), 694 (2016).
15. L. R. Solon, R. Aronson, and G. Gould, "Physiological Implications of Laser Beams," Science **134**(3489), 1506–1508 (1961).
16. M. M. Zaret, G. M. Breinin, H. Schmidt, H. Ripps, I. M. Siegel, and L. R. Solon, "Ocular lesions produced by an optical maser (laser)," Science **134**(3489), 1525–1526 (1961).
17. R. Henderson and K. Schulmeister, *Laser Safety* (CRC Press, 2003).
18. G. Giuliani, M. Norgia, S. Donati, and T. Bosch, "Laser diode self-mixing technique for sensing applications," J. Opt. A: Pure Appl. Opt. **4**(6), S283–S294 (2002).
19. M. Wang and G. Lai, "A self-mixing interferometer using an external dual cavity," Meas. Sci. Technol. **14**(7), 1025–1031 (2003).
20. Y. Zhao, M. Wang, J. Zhou, and X. Dai, "Self-Mixing Interference in Fiber Ring Laser With Parallel Dual-Channel," IEEE Photonics Technol. Lett. **21**(13), 863–865 (2009).
21. Y. Ruan, B. Liu, Y. Yu, J. Xi, Q. Guo, and J. Tong, "Improving Measurement Sensitivity for a Displacement Sensor Based on Self-Mixing Effect," IEEE Photonics J. **10**(6), 1–10 (2018).
22. L. Lu, W. Zhang, B. Yang, J. Zhou, H. Gui, and B. Yu, "Dual-Channel Self-Mixing Vibration Measurement System in a Linear Cavity Fiber Laser," IEEE Sens. J. **13**(11), 4387–4392 (2013).
23. V. Shusterman, P. Nagpal, D. Thedens, X. Zhu, D. S. Matasic, J. Y. Yoon, G. Morgan, S. Hoffman, and B. London, "Magnetic resonance imaging of contracting ultrathin cardiac tissue," Biomed. Phys. Eng. Express **5**(4), 045003 (2019).
24. L. Tirkkonen, H. Halonen, J. Hyttinen, H. Kuokkanen, H. Sievänen, A. M. Koivisto, B. Mannerström, G. K. B. Sándor, R. Suuronen, S. Miettinen, and S. Haimi, "The effects of vibration loading on adipose stem cell number, viability and differentiation towards bone-forming cells," J. R. Soc., Interface **8**(65), 1736–1747 (2011).
25. H. T. Halonen, J. A. K. Hyttinen, and T. O. Ihalainen, "Miniaturized Stimulator for Imaging of Live Cell Responses to High Frequency Mechanical Vibration," in *CMBEBIH 2019. IFMBE Proceedings*, vol 73, A. Badnjevic, R. Škrbić, and L. Gurbeta Pokvić, eds. (Springer, Cham, 2020), pp 21–27.
26. A. Kamgoué, J. Ohayon, Y. Usson, L. Riou, and P. Tracqui, "Quantification of cardiomyocyte contraction based on image correlation analysis," Cytometry **75A**(4), 298–308 (2009).
27. V. V. Vorobieva and P. D. Shabanov, "Vibration Model for Hypoxic Type of Cell Metabolism Evaluated on Rabbit Cardiomyocytes," Bull. Exp. Biol. Med. **147**(6), 768–771 (2009).
28. E. de Langre, "Plant vibrations at all scales: a review," J. Exp. Bot. **70**(14), 3521–3531 (2019).
29. B. Mortimer, A. Soler, L. Wilkins, and F. Vollrath, "Decoding the locational information in the orb web vibrations of Araneus diadematus and Zygiella x-notata," J. R. Soc., Interface **16**(154), 20190201 (2019).
30. R. Lang and K. Kobayashi, "External optical feedback effects on semiconductor injection laser properties," IEEE J. Quantum Electron. **16**(3), 347–355 (1980).
31. K. Petermann, *Laser Diode Modulation and Noise* (Kluwer Academic Publishers, 1988).
32. G. A. Acket, D. Lenstra, A. J. D. Boef, and B. H. Verbeek, "The influence of feedback intensity on longitudinal mode properties and optical noise in index-guided semiconductor lasers," IEEE J. Quantum Electron. **20**(10), 1163–1169 (1984).
33. C. H. Henry, "Theory of the linewidth of semiconductor lasers," IEEE J. Quantum Electron. **18**(2), 259–264 (1982).
34. T. Bosch, N. Servagent, and S. Donati, "Optical feedback interferometry for sensing application," Opt. Eng. **40**(1), 20–27 (2001).
35. S. Donati, "Responsivity and noise of self-mixing photodetection schemes," IEEE J. Quantum Electron. **47**(11), 1428–1433 (2011).
36. Z. Zhang, C. Li, and Z. Huang, "Vibration measurement based on multiple Hilbert transform for self-mixing interferometry," Opt. Commun. **436**, 192–196 (2019).